Statistical Assessment of the PolInSAR Coherence Set for Geophysical Media

Maxim Neumann[1,2], Marc Jäger[2], Laurent Ferro-Famil[1], and Andreas Reigber[3]

[1]SAPHIR Team, IETR Laboratory, University of Rennes 1, Campus de Beaulieu,
263 Avenue Général Leclerc, 35042 Rennes, France, e–mail: maxim.neumann@univ-rennes1.fr
[2]Computer Vision and Remote Sensing Group, Berlin University of Technology, Berlin, Germany
[3]German Aerospace Center (DLR), Microwave and Radar Institute, Wessling, Germany

Abstract

This paper introduces the polarimetric interferometric coherence set statistics taking into account the whole polarization state space. The first part of this paper is devoted to the analysis of the inner structure of polarimetric interferometric coherences – in form of coherence set geometry (the numerical range approach) and distribution (probability density function) in the complex plane. The second part deals with the assessment of physical parameter estimation methods by statistical inference using the coherence set statistics. In particular, the random volume over ground model with thermal and temporal decorrelation sources is considered. The presented methods are of importance for validation of techniques which utilize polarimetric interferometry and for understanding of the PolInSAR coherence properties.

1 Introduction

The interferometric SAR coherence is a parameter that is sensitive both to the volumetric structure of the scatterers in the resolution cell and to the temporal change processes. SAR polarimetry makes it possible to distinguish different kinds of scattering mechanisms in the same resolution cell. SAR polarimetry combined with SAR interferometry (PolInSAR) provides the possibility to observe the interferometric coherence at any arbitrary polarization state. The PolInSAR coherence set includes all possible coherences and, considered as a whole, can be related to the numerical range of the whitened and reduced coherency matrix. However, the observed PolInSAR coherence set is only one of the many realizations of the true coherence set and needs further statistical assessment in order to evaluate the confidence in the coherences and the accuracy of the parameter inversion techniques [1, 2].

This paper analyzes the coherence set geometry and statistics for geophysical media with distributed scattering characteristics. This implies a large number of scatterers, reflection symmetry (after terrain slope and squint angle corrections) and similarity of polarimetric responses at baseline ends. The last assumption is crucial for the coherence set geometry analysis, but is not required for the coherence set statistics.

In section 2, the PolInSAR coherence set is introduced. In 2.1, it is demonstrated how to extract coherence set geometry information from the numerical range. Coherence set statistics (i.e. statistics of the coherences over the whole polarization space, given the scattering covariance matrix) are presented in 2.2. In section 3, the coherence set of vegetation is examined. The vegetation is modeled by the random volume over ground (RVoG) model [3] with the additional thermal and temporal decorrelation sources (TT–RVoG).

2 Polarimetric Interferometric Coherence Set

The polarimetric interferometric scattering behavior can be represented by the true covariance matrix $\boldsymbol{\Sigma}$. However, this matrix cannot be directly observed and it is estimated from sample scattering vectors $\mathbf{k}_{1,2}$ by means of multi–looking ($\langle \ldots \rangle$):

$$\mathbf{C} = \langle \mathbf{k}\mathbf{k}^{\dagger} \rangle = \begin{bmatrix} \mathbf{C}_{11} & \mathbf{C}_{12} \\ \mathbf{C}_{12}^{\dagger} & \mathbf{C}_{22} \end{bmatrix}, \quad \text{with } \mathbf{k} = \begin{bmatrix} \mathbf{k}_1 \\ \mathbf{k}_2 \end{bmatrix}. \quad (1)$$

Assuming $\langle \mathbf{k}_1\mathbf{k}_1^{\dagger} \rangle \approx \langle \mathbf{k}_2\mathbf{k}_2^{\dagger} \rangle$ makes it possible to use the normalized matrix $\boldsymbol{\Pi}$,

$$\boldsymbol{\Pi} = \mathbf{C}_{11}^{-\frac{1}{2}} \mathbf{C}_{12} \mathbf{C}_{22}^{-\frac{1}{2}}, \quad (2)$$

for the computation of PolInSAR coherences directly:

$$\gamma_{(\boldsymbol{\omega})} = f_\gamma(\mathbf{C}, \boldsymbol{\omega}) = \frac{\boldsymbol{\omega}^{\dagger}\mathbf{C}_{12}\boldsymbol{\omega}}{\sqrt{\boldsymbol{\omega}^{\dagger}\mathbf{C}_{11}\boldsymbol{\omega}\,\boldsymbol{\omega}^{\dagger}\mathbf{C}_{22}\boldsymbol{\omega}}} \approx \mathbf{w}^{\dagger}\boldsymbol{\Pi}\mathbf{w}. \quad (3)$$

The numerical range of $\boldsymbol{\Pi}$, $\mathcal{W}(\boldsymbol{\Pi})$, provides the region of coherences in the complex plane [4, 5]:

$$\mathcal{W}(\boldsymbol{\Pi}) = \{\mathbf{x}^{\dagger}\boldsymbol{\Pi}\mathbf{x} : \mathbf{x} \in \mathbb{C}^q, \|\mathbf{x}\| = 1\} \quad (4)$$

where q is the dimensionality, i.e. the number of polarization channels. Similarly, we define the coherence set as the numerical range of $\mathbf{\Pi}$, but considering the distribution of polarizations:

$$\mathbf{\Gamma(C)} = \{\gamma_{(\omega)} : \omega \in \mathbb{C}^q, \omega \sim F(\omega)\} \qquad (5)$$
$$\approx \mathbf{\Gamma(\Pi)} = \{\omega^\dagger \mathbf{\Pi} \omega : \omega \in \mathbb{C}^q, \omega \sim F(\omega)\}$$
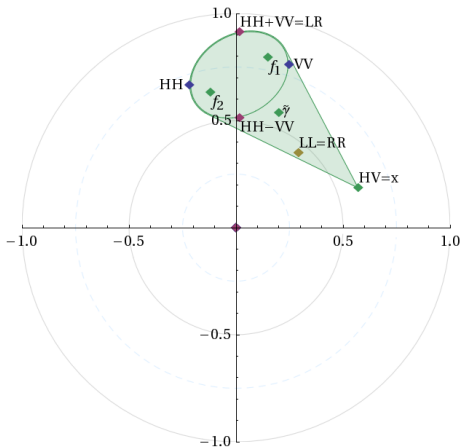
where $\omega \sim F(\omega)$ expresses that ω follows the distribution $F(\omega)$ of polarizations. The numerical range of a matrix is a projection of this matrix on the complex plane, without considerations about the density. Therefore, the numerical range contains information only about the geometry (shape and inner structure) of the coherence set, projected on the complex plane. While the coherence set contains additionally the probabilities of the coherences in the complex plane, and is suitable for statistical inference.

2.1 Coherence Set Geometry

Monostatic data with reflection symmetry results in the following structure of the $\mathbf{\Pi}$ matrix [5]

$$\mathbf{\Pi} = \begin{bmatrix} \gamma_{11} & \rho_{12} & 0 \\ \rho_{21} & \gamma_{22} & 0 \\ 0 & 0 & \gamma_{33} \end{bmatrix} = \mathcal{E} \oplus x = \tilde{\gamma}\mathbf{I} + \mathcal{E}' \oplus x' \quad (6)$$

where $\mathcal{E}$ is the 2×2 linearly co–polarized coherence ellipse matrix, x the cross–polarized coherence, and $\tilde{\gamma} = \frac{1}{3}\text{trace}\,\mathbf{\Pi}$ the center of the coherence set. In case of a uniform distribution of polarizations $F(\omega)$, $\tilde{\gamma}$ is the maximum likelihood estimator of the mean coherence over all polarizations. $\mathcal{E}'$ and x' are given relative to the center position $\tilde{\gamma}$. The whole coherence set shape is formed as the convex hull over $\mathcal{E}$ and x, as shown on an example in Fig. 1. The eigenvalues of $\mathcal{E}$ provide the foci f_1, f_2 of the ellipse, and the whole spectrum of $\mathbf{\Pi}$ is given by $\{f_1, f_2, x\}$.

Figure 1: An example of a general coherence set geometry for a monostatic acquisition with reflection symmetry.

2.2 Coherence Set Statistics

To analyze the distribution of PolInSAR coherences in the complex plane, it will prove useful to derive the marginal probability of the complex coherence with respect to the polarization state. But prior to this, one needs to define the joint distribution of the complex coherence and the transmit/receive polarizations. The state of the wave polarization can be described by the orientation and ellipticity angles Ψ, χ of the polarization ellipse ($0 \leq \Psi \leq \pi$, $-\frac{\pi}{4} \leq \chi \leq \frac{\pi}{4}$), which provide the spherical coordinates of polarization state on the unitary wave Poincaré sphere. The state of the scattering polarization is then given by the combination of the transmit and receive wave polarization angles ($\psi = \begin{bmatrix} \Psi_r\ \chi_r\ \Psi_t\ \chi_t \end{bmatrix}^T$), which determine the scattering polarization vector $\omega = \omega(\psi)$.

Using the Bayes' theorem, the joint probability density function (PDF) of the sample coherence ($\gamma = de^{i\phi}$) and the polarization angles vector ψ_ξ, which determines the true coherence $\xi = De^{i\beta} = f_\xi(\mathbf{\Sigma}, \omega(\psi_\xi))$, can be expressed by

$$p(\gamma, \psi_\xi | \mathbf{\Sigma}, L) = p(\gamma|\psi_\xi, \mathbf{\Sigma}, L)\, p(\psi_\xi). \qquad (7)$$

This PDF can be interpreted as the joint probability of the sample and the true coherence, γ and $\xi_{(\psi_\xi)}$, for a single polarization.

The conditional probability density for the coherence, given the true coherence, has been derived in [6]:

$$p(\gamma|\psi_\xi, \mathbf{\Sigma}, L) = p(\gamma|\xi_{(\psi_\xi)}, L) = \frac{(1-D^2)^L}{\pi\Gamma(L)\Gamma(L-1)}$$
$$d(1-d^2)^{L-2} \left[\Gamma^2(L)\,_2F_1(L,L;1/2, d^2D^2\cos^2(\phi-\beta)) \right.$$
$$+ 2\Gamma^2(L+1/2)dD\cos(\phi-\beta)$$
$$\left. _2F_1(L+1/2, L+1/2;3/2; d^2D^2\cos^2(\phi-\beta)) \right] \quad (8)$$

where L is the effective number of looks (ENL), Γ is the Gamma function, and $_2F_1$ is the Gauss's Hypergeometric function. This PDF is the "usual" single–pol coherence PDF.
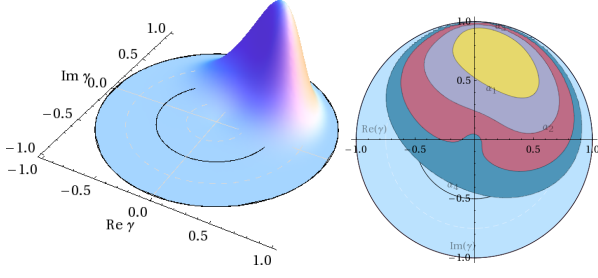
The density of scattering polarizations is determined by the assumption of joint uniform distribution of polarization angles in their domains.

The marginal probability of the complex coherence, which represents the coherence density over all polarizations, is obtained by integrating (7) over the polarization space:

$$p(\gamma|\mathbf{\Sigma}, L) = \iiiint p(\gamma|\xi_{(\psi_\xi)}, L)p(\psi_\xi)d\psi_\xi. \quad (9)$$

With similar reasoning one can derive the expression for the a–posteriori PDF of the true coherence, given the sample covariance matrix and assuming (in the absence of better knowledge) a uniform prior distribution:

$$p(\xi|\mathbf{C}, L) = \iiiint \left[\iint p(\gamma_{(\psi_\gamma)}|\xi', L)d\xi' \right]^{-1}$$
$$p(\gamma_{(\psi_\gamma)}|\xi, L)p(\psi_\gamma)d\psi_\gamma \quad (10)$$

Figure 2: Coherence set probability density function with confidence regions at confidence levels α_i, $i \in \{1, 2, 3, 4\}$.

where the outer integral is taken over the scattering polarization state domain, and the inner, representing the marginal data PDF, is taken over the complex coherence domain, i.e. over the amplitude and phase of the unitary disc in the complex coherence plane.

No analytical forms for the integrals (9) and (10) can be given at the moment and they need to be solved numerically. For the example coherence set from Fig. 1, the marginal PDF with respect to polarization states is presented in Fig. 2, using 9 looks. On the right side, the confidence regions are visualized for the given distribution corresponding to confidence levels $\alpha_i = 1 - \mathrm{erf}(i/\sqrt{2})$, for $i \in \{1, 2, 3, 4\}$, where erf() is the error function (i.e. $1 - \alpha_i \in \{68.27\%, 95.45\%, 99.73\%, 99.994\%\}$).

3 Vegetation Model Assessment

3.1 TT–RVoG Coherence Model

In order to examine the coherence set variance on more realistic examples, the classical RVoG [3] coherence model with thermal and temporal decorrelation sources (TT–RVoG) is considered:

$$\gamma_{(\boldsymbol{\omega})} = \gamma_{therm(\boldsymbol{\omega})} \left(c_{g(\boldsymbol{\omega})} \gamma_{gr} + (1 - c_{g(\boldsymbol{\omega})}) \gamma_{vol} \gamma_{temp} \right) \tag{11}$$

where $c_{g(\boldsymbol{\omega})} = \frac{m_{(\boldsymbol{\omega})}}{m_{(\boldsymbol{\omega})}+1}$ is the relative ground contribution, and m is the ground–to–volume ratio. The decorrelation sources are given by

$$\gamma_{therm} = \frac{1}{1 + \frac{1}{SNR_{(\boldsymbol{\omega})}}}, \quad \gamma_{gr} = e^{i\phi_0}, \tag{12}$$
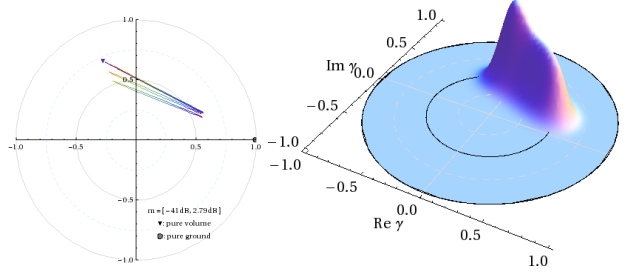
$$\gamma_{vol} = e^{i\phi_0} \int_0^{h_V} e^{ik_z z} f(z) dz, \quad f(z) = \frac{e^{\frac{2\sigma z}{\cos \theta_0}}}{\int_0^{h_V} e^{\frac{2\sigma z'}{\cos \theta_0}} dz'}, \tag{13}$$

$$\gamma_{temp} = \gamma_{Brown} = e^{-\sigma_B^2 t/2}, \quad \sigma_B^2 = \frac{s_B^2 k^2}{[\text{time unit}]}. \tag{14}$$

These are the thermal, ground, volume, and temporal decorrelations. SNR is the signal–to–noise ratio, ϕ_0 the ground phase, k_z the vertical wavenumber, h_V the vegetation height, σ the extinction due to wave propagation in the vegetation, θ_0 the incidence angle, and k the wavenumber. The temporal decorrelation is assumed to be due to Brownian motion of volume particles, where σ_B^2 is the variance

Figure 3: The true coherence set and the PDF (49 looks) for the RVoG scenario. The color represents the ground–to–volume ratio m from -41dB (red) to 2.8dB (violet).

Figure 4: The true coherence set and the PDF (49 looks) for the TT–RVoG scenario. Additionally, the coherence set of the pure RVoG and RVoG with thermal decorrelation is presented on the left figure.
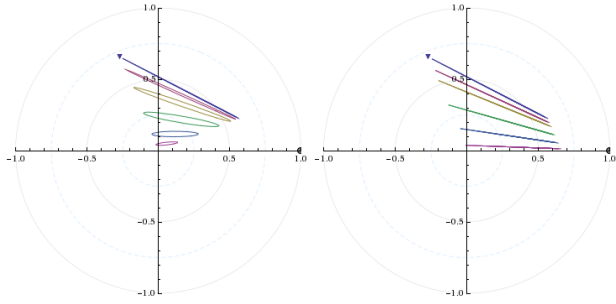
per time unit, related to s_B^2 which is the range variance of the vegetation particles in the direction of propagation.

3.2 Modeled Scenario

The example scenario is simulated as a random volume of needle–like particles over a relatively smooth ground, without under–storeys or slopes. Vegetation height is $h_v = 20$m, vegetation density causes an extinction of $\sigma = 0.3$dB/m, the acquisition system geometry is described by the vertical wavenumber of $k_z = 0.15$/rad. The ground–to–volume intensity ratio varies between -41dB and 2dB. The SNR varies for all polarizations between 9dB and 15dB. The time span between acquisitions is 1 day (24 hours). The temporal decorrelation of the volume is assumed to follow the distribution for Brownian motion, with a particle motion standard deviation of 0.002m per hour (0.26mm/min).

3.3 Observations

Figs. 3 and 4 show the coherence set and the a–priori PDFs (49 looks) for the RVoG and the TT–RVoG scenarios. Fig. 5 demonstrates the behavior of the coherence set under varying thermal or temporal decorrelations. The thermal decorrelation destroys the line structure, since it is not only a factor, but also a function of polarization. With increasing temporal decorrelation, the observed coherence corresponding to the volume decreases. Simultaneously, the relative ground contribution in the total coherence increases,

Figure 5: Influence of thermal and temporal decorrelation on the RVoG coherence set. Left: The disintegration of the line structure with lower (polarization dependent) SNR values. The mean SNR for the different scenarios varies from top to bottom: ∞dB (only RVoG decorrelation), 15dB, 10dB, 5dB, 0dB, -5dB. Right: Temporal decorrelation due to Brownian motion of the volume scatterers as a function of time. SDEV of scatterer movements in the line of sight: 2mm/hour. From top to bottom: 0h (only RVoG), 1 day, 2 days, 5 days, 10 days, 20 days.
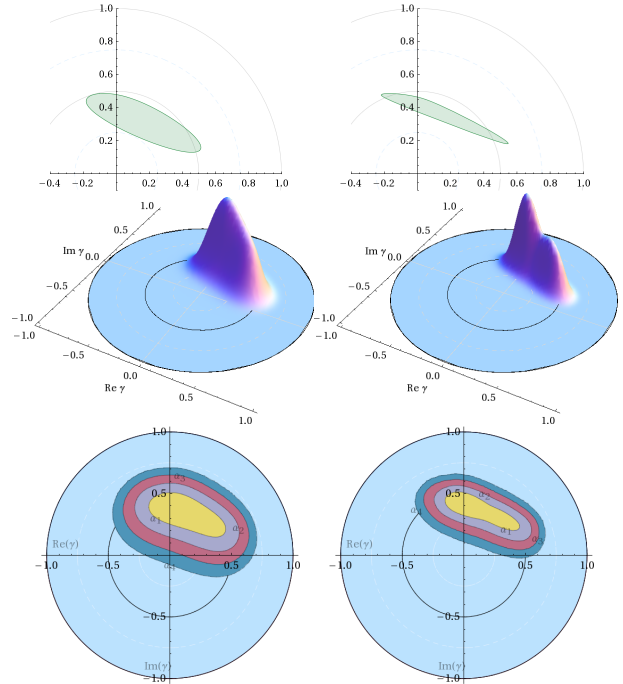
and the coherences with high ground–to–volume ratio increase even in their magnitude. With the given decorrelation rate, the volume decorrelates completely after about 20 days, while scatter response from the ground increases its coherence. In case of total temporal decorrelation of the volume, the total coherence is given by $\gamma_{therm}\gamma_{gr}c_g$. In this case the coherence shape corresponds to the pure ground, simply decreased in magnitude by the factor c_g because of the present totally uncorrelated volume.

Fig. 6 presents two sample coherence sets with 49 and 100 looks and the obtained a–posteriori PDFs with confidence regions. As can be seen, the confidence regions of the sample realizations enclose the true coherence set, which is expected, since the sample distributions follow the true one.

3.4 Discussion

The next objective is to apply the coherence set geometry and statistics approaches to the analysis of real data. When dealing with real data, one has to assure a high degree of homogeneity of the scene. Also, to note is the increased amount of samples required for the same ENL. Frequently, the data is oversampled and, moreover, even a small heterogeneity leads to a decreased ENL.

The presented study can be extended to accurate statistical error analysis of parameter estimation methods. It is also a first step towards statistical enhancement of PolInSAR parameter inversion techniques, with the goal of fitting estimated coherence set samples to modeled coherence set geometries and densities. In the near future, a comparison of real data with the models, which are assumed to approximate the environment, could be possible and beneficial. An additional goal is the development of statistical tests for determining (accepting or rejecting) the appropriate model for parameter inversion for a given real scene.

Figure 6: From top to bottom: sample coherence sets, a–posteriori PDFs, and a–posteriori confidence regions for the TT–RVoG scenario with 49 (left) and 100 (right) looks.

4 Conclusion

In this paper we discussed methods for analysis of the PolInSAR coherence. Two approaches have been utilized to combine the full polarization space and the interferometric coherence. The numerical range concept provides the possibility to analyze the geometry of the coherences, projected onto the complex plane. Coherence set statistics have been examined on the example of a vegetation coherence model. The presented methods can prove useful for validation of PolInSAR applications which intend to use the whole polarization state and coherence space.

References

[1] G. Krieger, K. P. Papathanassiou, and S. R. Cloude. Spaceborne Polarimetric SAR Interferometry: Performance Analysis and Mission Concepts. *EURASIP Journal of Applied Signal Processing*, 20:3272–3292, 2005.

[2] O. Stebler. *Analyse der komplexen Kohaerenz flugzeug- und satellitengestuetzter InSAR-Systeme als Funktion konventioneller und interferometrisch optimierter Polarisationszustaende*. PhD thesis, University of Zurich, 2004.

[3] K. P. Papathanassiou and S. R. Cloude. Single–Baseline Polarimetric SAR Interferometry. *IEEE Trans. Geosci. Remote Sensing*, 39:2352–2363, November 2001.

[4] E. Colin. A Mathematical study about the "Coherence Set" in Polarimetric Interferometry. In *Proc. EUSAR*, Dresden, Germany, May 2006.

[5] M. Neumann, A. Reigber, and L. Ferro-Famil. POLInSAR Coherence Set Theory and Application. In *Proc. EUSAR*, Dresden, Germany, May 2006.

[6] R. Touzi, A. Lopes, J. Bruniquel, and P. W. Vachon. Coherence Estimation for SAR Imagery. *IEEE Trans. Geosci. Remote Sensing*, 37(1):135–149, January 1999.